Upconverted excitation energy lock-in for deep-ultraviolet enhancement

Qianqian Su
E401C, 99 Shanghai University, Baoshan https://orcid.org/0000-0002-8706-6760
Han-Lin Wei
Shanghai University
Shuai Wang
Shanghai University
Chaohao Chen
Institute for Biomedical Materials and Devices (IBMD), Faculty of Science, University of Technology Sydney, NSW 2007 https://orcid.org/0000-0003-4620-7771
Guan Ming
Southern University of Science and Technology
Yan Su
Genome Institute of Singapore
Haifang Wang
Shanghai University
Zhigang Chen
Donghua University
Dayong Jin (dayong.jin@uts.edu.au)
University of Technology Sydney https://orcid.org/0000-0003-1046-2666

Article

Keywords: Photo Upconversion of Near-infrared Irradiation, Heterogeneous Core-multishell Nanostructure, Interior Energy Traps, Cascade Sensitizations

Posted Date: October 28th, 2020

DOI: https://doi.org/10.21203/rs.3.rs-88155/v1

Version of Record: A version of this preprint was published at Nature Communications on July 16th, 2021. See the published version at https://doi.org/10.1038/s41467-021-24664-x.

Abstract

Photon upconversion of near-infrared (NIR) irradiation into deep-ultraviolet (UV) emission offers many exciting opportunities for drug release in deep tissues, photodynamic therapy, solid-state lasing, energy storage, and photocatalysis. However, NIR-to-deep-UV upconversion remains a daunting challenge due to low quantum efficiency. Here, we report an unusual six-photon upconversion process in Gd3+/Tm3+-codoped nanoparticles comprising a heterogeneous, core-multishell nanostructure. This multishell design efficiently suppresses energy consumption induced by interior energy traps, maximizes cascade sensitizations of the NIR excitation, and promotes upconverted deep-UV emission from high-lying excited states. We released the intense six-photon-upconverted UV emissions at 253 nm under 808-nm excitation. This work provides new insight into mechanistic understanding of the upconversion process within the heterogeneous architecture, while offering exciting opportunities for developing nanoscale deep-UV emitters that can be remotely controlled in deep tissues upon NIR illumination.

Introduction

Multiphoton upconversion processes that convert NIR excitation into visible emissions have attracted considerable attention owing to broad technical applications of anti-Stokes shifts[1-6]. Though UV upconversion luminescence can be a powerful tool for applications in biomedical[7-9], environmental[10,11], and industrial fields[12,13], their practical implementations have been hindered by low emission intensities and difficulties in achieving large shifts into the deep-UV region. NIR-to-deep UV upconversion is significantly influenced by many deleterious factors, such as concentration quenching, surface quenching, cross-relaxation between lanthanide ions, and competitive energy harvesting from low-lying energy levels.

Attempts have been made to enhance the emission intensity in the UV range, for instance, by controlling the particle phase and size[14], the pulse width of excitation beams[15], dopant composition[16], and nanoparticle core-shell structures[12,17-19]. However, severe cross-relaxation between lanthanide ions and unwanted energy consumption by interior and surface quenchers drastically depopulates the excited states at high-lying emitting levels, thus mitigating upconverted UV emission[20].

Deep-UV upconversion emission is particularly useful for drug release in deep tissues, since NIR excitation penetrates deeper through tissue than visible light and localized UV generation can trigger drug release with high spatial and temporal precisions[21-25]. Compared with Yb^{3+}-sensitized upconversion nanoparticles (UCNPs), Nd^{3+}-sensitized UCNPs offer deep penetration depths and minimal over-heating effect, owing to low coefficients of water absorption under 800-nm excitation[26]. Despite enticing prospects, deep-UV emission from Nd^{3+}-sensitized UCNPs has been challenging because of densely packed excited states of Nd^{3+} and dominant cross-relaxation within the nanoparticle systems[27,28].

Here we report significantly enhanced UV upconversion emission through Nd^{3+} sensitization by controlling upconverted excitation energy flux within Gd^{3+}/Tm^{3+} codoped, core-multishell nanostructures. Our mechanistic investigation reveals upconverted excitation lock-in (UCEL) mode in which Gd^{3+}-sensitized excitation energy can be retained by using an optical inert $NaYF_4$ interlayer. This nanostructure preserves the upconversion energy within the core domain and effectively suppresses energy dissipation by interior traps, enabling six-photon-upconverted UV emission at 253 nm under 808-nm excitation.

Results

Heterogeneous nanostructural design. In our experiment, we designed a heterogeneous core-multishell structure to suppress surface quenching and achieve tunable emissions. In a conventional design[29,30], under 808-nm excitation, Nd^{3+} sensitizers harvest excitation photons and subsequently pass them to Yb^{3+} ions with an excited state at ~ 10,000 cm^{-1}. Energy migration through a network of high concentration Yb^{3+} ions promotes back-energy transfer of the NIR excitation to Tm^{3+} emitters with ladder-like metastable intermediate states, facilitating sequential upconversion processes from NIR to visible/UV. By doping of Gd^{3+}, upconverted UV emission from high-lying states of Tm^{3+} can be further transferred to Gd^{3+} ions as deep-UV energy reservoirs.

The key to our design is the optical inert $NaYF_4$ layer locating in the first shell layer of $NaGdF_4$:Yb,Tm@ $NaGdF_4$:Yb@$NaGdF_4$:Yb,Nd@$NaGdF_4$ (Gd-$CS_{Gd}S_2S_3$) nanoparticle (Scheme 1). This inert layer can lock-in the upconverted excitation energy of Gd^{3+} ions. The Gd^{3+} network can reuse the upconverted excitation energy and prevent depopulation by deleterious energy traps within the nanoparticles. The $NaYF_4$ layer plays a key role in interdicting detrimental energy transfer between Gd^{3+} and interior traps, enhancing five- and six-photon-upconverted UV emissions.

Upconverted excitation lock-in (UCEL) mode. The UCEL mode requires both an optical inert $NaYF_4$ interlayer and a network of Gd^{3+} ions to recycle upconversion energy for deep-UV emission amplification. Fig. 1 illustrates a typical upconversion process in heterogeneous, core-multishell nanoparticles upon 808-nm excitation. In brief, 808 nm photons are first sensitized by Nd^{3+} sensitizer ions, being populated at the $^4F_{5/2}$ energy state and quickly relaxed to the $^4F_{3/2}$ energy state of Nd^{3+}. The excited Yb^{3+} ions serve as an energy migrator to populate the $^3P_2$ state of Tm^{3+} through a five-photon upconversion process. The ^6D_J state of Gd^{3+} is further populated by the appropriate energy matching of the following transitions of Tm^{3+}: $^3P_{0,1}\rightarrow{}^1D_2$ (~7600 cm^{-1}, ~8200 cm^{-1}), $^3F_{2,3}\rightarrow{}^3H_5$ (~6700 cm^{-1}, ~6200 cm^{-1}), and $^1G_4\rightarrow{}^3H_4$ (~8600 cm^{-1}), via an energy transfer process[31]. However, the probability of nonradiative relaxation of $^6I_J\rightarrow{}^6P_J$ is larger than that of the radiative transition of $^6I_J\rightarrow{}^8S_{7/2}$, resulting in an efficient population of the $^6P_{7/2}$ state, commonly observed in Gd-based homogeneous nanostructures[18]. In our design, the $NaYF_4$-based

first shell layer selectively blocks the energy transfer from Gd^{3+} to interior energy traps (e.g., lattice defects and impurities). It preserves and recycles the excitation energy within the core region, leading to increased populations in the ^6D_J, ^6I_J, and ^6P_J states of Gd^{3+} and intense UV emission of Gd^{3+}.

Controlled synthesis. We used a layer-by-layer epitaxial growth method[20] to synthesize a batch of Gd-$CS_YS_2S_3$ nanoparticles with optimized concentrations of co-dopants[30] following the design of $NaGdF_4$:49%Yb,1%Tm@$NaYF_4$:20%Yb@$NaGdF_4$:10%Yb,50%Nd@$NaGdF_4$ (Fig. 2a). Transmission electron microscopy (TEM) images of obtained Gd-$CS_YS_2S_3$ nanoparticles show the average size of ~29 nm with each layer ~2.5 nm in thickness (Supplementary Fig. S1). High-resolution TEM shows the single-crystalline structure of the as-synthesized core-multishell nanoparticles (Fig. 2b inset), and X-ray powder diffraction result (XRD, JCPDS file number 27-0699, Supplementary Fig. S2) confirms the hexagonal phase of the as-prepared nanoparticles. High-angle annular darkfield scanning TEM identified the formation of the heterogeneous core-multishell structures (Fig. 1b), in which the brighter regions correspond to heavier elements (Gd, Yb, and Nd) and the darker parts correspond to lighter ones (Y). Energy-dispersive X-ray mapping analysis further confirmed the heterogeneous core-multishell structures (Fig. 1c, Supplementary Fig. S3).

Remarkable deep-UV enhancement. To investigate the unusual deep-UV upconversion emission from Gd^{3+}, we recorded the photoluminescence spectra of the as-synthesized nanoparticles at room temperature. Usually, in favor of the lower $^6P_{7/2}$ (311 nm) energy level, the Gd^{3+} emission in the deep-UV range is quenched, and optical transitions of (^6D_J, ^6I_J, $^6P_{5/2}\rightarrow{}^8S_{7/2}$) could hardly be spectroscopically detected (Supplementary Figs. S4-7)[12]. In contrast, as shown in Fig. 1c and Supplementary Fig. S8, intense upconversion emissions from ^6D_J and ^6I_J of Gd^{3+} peaked at 253 nm ($^6D_{9/2}\rightarrow{}^8S_{7/2}$), 273 nm ($^6I_J\rightarrow{}^8S_{7/2}$), 276 nm ($^6I_J\rightarrow{}^8S_{7/2}$), 279 nm ($^6I_J\rightarrow{}^8S_{7/2}$), 306 nm ($^6P_{5/2}\rightarrow{}^8S_{7/2}$) and 311 nm ($^6P_{7/2}\rightarrow{}^8S_{7/2}$) in the UV region were observed either under 808 nm or 980 nm excitation. Moreover, we observed more than 50-fold and 30-fold enhancements in Gd^{3+} emission (311 nm) by our Gd-$CS_YS_2S_3$ heterogeneous core-multishell design compared with the conventional Gd-$CS_{Gd}S_2S_3$ nanoparticles under 808 nm and 980 nm excitation, respectively (Supplementary Figs. S9 and S10), although the absorption profile of Gd-$CS_YS_2S_3$ is not changed compared with that of Gd-$CS_{Gd}S_2S_3$ nanoparticles (Supplementary Fig. S11). As verified by the emission spectra of several different batches of as-prepared nanoparticles (Supplementary Fig. S12), our protocol to enhance the deep-UV upconversion emissions is reproducible.

We further studied the excitation power dependence of luminescence intensity from higher-lying ^6D_J, ^6I_J and ^6P_J excited states of Gd^{3+} (Fig. 2f). The number of photons (n) required to populate the upper emitting state can be calculated by the luminescence intensity I_f and the pump power of laser P following

relation of $I_f \propto P^{n32}$. The output slope for 253 nm emission band was calculated as 5.92, indicating that six 808 nm photons needed to populate the ^6D_J level, following a six photon upconversion process (Fig. 2g), while *n* values obtained for 276 and 311 nm emissions were 5.07 and 5.09, indicating five-photon processes (Fig. S13).

Gd^{3+} energy recycling above ^6P_J. To probe the role of $NaYF_4$ layer in locking-in and recycling Gd^{3+} excitation energy, we have compared the excited state lifetime of Gd^{3+}. As shown in Fig. 3 and Supplementary Fig. S14, a significant prolonged (~4 times) lifetime of Gd^{3+} emission from the $^6P_{7/2}$ level was achieved when the $NaYF_4$ first layer was applied. In contrast, there were negligible changes in the Gd^{3+} lifetimes for emissions from ^6D_J and ^6I_J energy levels, indicating the energy loss from Gd^{3+} to interior energy traps was mainly through $^6P_{7/2}$ energy level of Gd^{3+} due to small energy gap between ^6D_J, ^6I_J and ^6P_J (Supplementary Fig. S15). In addition, the emission intensities of Nd^{3+} at 893 nm ($^4F_{3/2} \rightarrow {}^4I_{9/2}$), 1057 nm ($^4F_{3/2} \rightarrow {}^4I_{11/2}$), and 1330 nm ($^4F_{3/2} \rightarrow {}^4I_{13/2}$) and Tm^{3+} at ~1460 nm ($^3H_4 \rightarrow {}^3F_4$) in the near-infrared range were essentially unaltered (Supplementary Fig. S16). These results indicate that the $NaYF_4$-assisted UCEL mechanism favors the upconversion emissions from high-lying energy levels.

The role of the first layer of $NaYF_4$ shell. To further verify the role of $NaYF_4$ layer in enhancing the deep-UV emissions, we synthesized a group of Gd-$CS_YS_2S_3$, Gd-$CS_1S_YS_3$ and Gd-$CS_1S_2S_Y$ heterogeneous nanoparticles, in which $NaGdF_4$ was selectively replaced by $NaYF_4$ host lattice in the first, second and third layer, respectively (Fig. 4a). The intense deep UV emission was only observed in Gd-$CS_YS_2S_3$ nanoparticles. The emission profiles of Gd-$CS_1S_YS_3$ and Gd-$CS_1S_2S_Y$ were quite similar to Gd-$CS_{Gd}S_2S_3$ nanoparticles. Moreover, when the optically inert Y^{3+} ions in the first layer were replaced by half of the Gd^{3+} ions, a drastic reduction of the Gd^{3+} emission was observed, indicating that the optical inert $NaYF_4$ layer can effectively prevent the back energy transfer from Gd^{3+} (Supplementary Fig. S17).

We further prepared a group of Gd-$CS_YS_2S_3$ nanoparticles doped with Tb^{3+} or Eu^{3+} ions in the first layer (Gd-$CS_{Y\text{-}15\%Tb}S_2S_3$ or Gd-$CS_{Y\text{-}15\%Eu}S_2S_3$), which can extract the excitation energy from Gd^{3+} to emit green and red upconversion emissions through the scheme of energy migration upconversion (EMU)[18]. Upon excitation at 808 nm, the characteristic emissions of Tb^{3+} and Eu^{3+} (highlighted in color) were observed (Fig. 4b-c and Supplementary Fig. S18), but no enhancement in deep-UV emission. Doping with 15% Tb^{3+} or Eu^{3+} in the outmost layer only led to weak emission of Tb^{3+} or Eu^{3+} (Supplementary Fig. S19). The weak Tb^{3+} and Eu^{3+} emissions were attributed to the interior energy trapping of the excitation energy in the Gd^{3+} sublattice. Together, these results indicate that an efficient energy transfer pathway

(Nd^{3+}→Yb^{3+}→Tm^{3+}→Gd^{3+}) occurs[33], and the excitation energy of Gd^{3+} can be easily dissipated through the emission of Tb^{3+}, Eu^{3+}, or interior traps without the $NaYF_4$ first-shell layer.

Determination of the interior traps. An efficient energy transfer can occur between Gd^{3+} and Nd^{3+} ions[34]. However, in our design, the energy transfer between these two ions did not happen. To preclude the possibility of the interior Nd^{3+} energy trapping, we prepared a series of Gd-$CS_{Gd}S_2S_3$ nanoparticles with and without Nd^{3+} dopant (Gd-$CS_{Gd}S_{50\%Nd}S_3$ and Gd-$CS_{Gd}S_{0\%Nd}S_3$). The lifetimes of Gd^{3+} (^6D_J, ^6I_J, ^6P_J) and Tm^{3+} ($^1I_6$, $^1D_2$) were virtually unchanged after removing Nd^{3+} dopants in nanoparticles (Fig. 4d and Supplementary Fig. 20). These results confirm that intense deep-UV emission from Gd^{3+} is enabled by obstructing the energy transfer from Gd^{3+} to interior lattice defects or impurities.

Furthermore, we compared the amount of light-to-heat conversion in Gd-$CS_YS_2S_3$ and Gd-$CS_{Gd}S_2S_3$ nanoparticles by using an infrared thermal imaging camera. As a higher concentration of Nd^{3+} in nanoparticles would generate more heat under single-beam infrared laser excitation[35], we measured the concentrations of Nd^{3+} in these two types of nanoparticles (Supplementary Table 1). The measured temperature rises of the solution of Gd-$CS_YS_2S_3$ and Gd-$CS_{Gd}S_2S_3$ are 5.0 ^oC and 7.2 ^oC under irradiation at 808 nm light, 1.9 ^oC and 3.2 ^oC under irradiation at 980 nm light, respectively (Fig. 5). These results suggest that less excitation energy is converted to lattice heating in heterogeneous core-multishell structures than in conventional nanoparticles.

Enhancement in highly doped single nanoparticles. To further evaluate UCEL mode in enhancing the high-order upconversion emissions in the heterogenous core-multishell structures, we implemented the similar design in the highly doped UCNP core, e.g. Gd-$C_{8\%Tm}S_YS_2S_3$ and Gd-$C_{8\%Tm}S_{Gd}S_2S_3$, and quantify the brightness of single UCNPs using a purpose-built confocal microscopy system (see Supplementary Fig. S21). Due to the significant UV absorption by the optical components, including the objective lens and mirrors, instead of a direct quantification of the deep UV emissions at a single nanoparticle level, we monitored the amount of the blue band emissions from a single nanoparticle. Under the same excitation power from both 808 nm and 976 nm lasers, the emission intensities of Gd-$C_{1\%Tm}S_YS_2S_3$ and Gd-$C_{1\%Tm}S_{Gd}S_2S_3$ nanoparticles under the 808 nm excitation were ~4 times and ~5 times higher than those under the 976 nm excitation, respectively (Supplementary Fig. S22). In contrast, much higher enhancement factors of the highly doped Gd-$C_{8\%Tm}S_YS_2S_3$ (~25 times) and Gd-$C_{8\%Tm}S_{Gd}S_2S_3$ (~15 times) nanoparticles were achieved under the 808 nm v.s. 976 nm excitations. These results suggest UCEL mode could be broadly applied to a variety of UCNP core concentrations[36] and under a large dynamic range of excitation power densities[37], suitable for both ensemble and single nanoparticle applications[38].

Discussion

In this study, we demonstrated an UCEL approach through the core-multishell heterogeneous structure design to regulate the energy transfer pathway in lanthanide-doped UCNPs for deep UV generation by 808 nm excitation. The key to this design is the utilization of an optical inert $NaYF_4$ interlayer between multiple cascade NIR photon sensitization shells and emitting core. Therefore, the sensitized NIR excitation energies can be transferred inbound and upconverted at the core domain of $NaGdF_4$:Yb,Tm, where high-concentration Gd^{3+} ions can recycle among the higher-lying excited energy states above ^6P_J to realize intense deep UV upconversion emissions. We believe this approach will advance the design rationale for enhancing the NIR sensitized deep UV upconversion emissions towards the potential areas of biomedicine, information technology, photocatalysis, environmental science and many other emerging fields.

Online Content Methods, along with any additional Extended Data display items and Source Data, are available in the online version of the paper; references unique to these sections appear only in the online paper.

Declarations

Acknowledgements The authors thank the National Natural Science Foundation of China (Nos. 21701109 and 31771105), the National Basic Research Program of China (No. 2016YFA0201600), Shanghai Shuguang Program (18SG29) and Natural Science Foundation of Shanghai (18ZR1401700) for financial supports. The authors acknowledge the assistance of SUSTech Core Research Facilities. The authors thank Prof. X. Liu, Prof. A. Cao, Dr. S. Han and Dr. J. Zhou for helpful discussion.

Author contributions Q.S. and D.J. conceived the project. Q.S., H.W. and D.J. designed the experiments and supervised the research. Q.S., H.L.W., S.W., C.C., M.G., and Z.C. were primarily responsible for the experiments of nanoparticles synthesis and characterization. Q.S., D.J., H.L.W., S.W., C.C., Y.S. and H.W. contributed to the data analyses and discussion. Q.S. and D.J. prepared figures and wrote the paper with input from other authors.

Author Information Reprints and permissions information is available online at http://www.nature.com/reprints. The authors declare no competing financial interests. Readers are welcome to comment on the online version of the paper. Correspondence and requests for materials should be addressed to Q.S. (chmsqq@shu.edu.cn), H.W. (hwang@shu.edu.cn), or D.J. (dayong.jin@uts.edu.au). These authors contributed equally: Qianqian Su, Han-Lin Wei.

References

1. Auzel, F. Upconversion and anti-stokes processes with f and d ions in solids. *Rev.* **104**, 139–174 (2004).
2. Bünzli, J.-C. G. & Piguet, C. Taking advantage of luminescent lanthanide ions. *Soc. Rev.* **34**, 1048–-1077 (2005).
3. Dong, H., Sun, L. D. & Yan, C. H. Energy transfer in lanthanide upconversion studies for extended optical applications. *Soc. Rev.* **44**, 1608–1634 (2015).
4. Wen, S., Zhou, J., Schuck, P. J., Suh, Y. D., Schmidt, T. W. & Jin, D. Future and challenges for hybrid upconversion nanosystems. *Photonics* **12**, 828–838 (2019).
5. Bettinelli, M., Carlos, L. D. & Liu, X. Lanthanide-doped upconversion nanoparticles. *Today* **68**, 38–44. (2015).
6. Su, Q., Feng, W., Yang, D. & Li, F. Resonance energy transfer in upconversion nanoplatforms for selective biodetection. *Chem. Res.* **50**, 32–40 (2017).
7. Jalani, G., Naccache, R., Rosenzweig, D. H., Haglund, L., Vetrone, F. & Marta Cerruti. Photocleavable hydrogel-coated upconverting nanoparticles: a multifunctional theranostic platform for NIR imaging and on-demand macromolecular delivery. *Am. Chem. Soc.* **138**, 1078–1083 (2016).
8. Yao, C. et al. Near-infrared-triggered azobenzene-liposome/upconversion nanoparticle hybrid vesicles for remotely controlled drug delivery to overcome cancer multidrug resistance. *Mater.* **28**, 9341–9348 (2016).
9. Zhang, Z. et al. Upconversion superballs for programmable photoactivation of therapeutics. *Commun.* **10**, 4586 (2019).
10. Gao, W., Zhang, W. & Lu, G. A two-pronged strategy to enhance visible-light-driven overall water splitting via visible-to-ultraviolet upconversion coupling with hydrogen-oxygen recombination inhibition. *Catal. B-Environ.* **212**, 23–31 (2017).
11. Anwer, H. & Park J. W. Near-infrared to visible photon transition by upconverting $NaYF_4$: Yb^{3+}, Gd^{3+}, Tm^{3+}@Bi_2WO_6 core@shell composite for bisphenol A degradation in solar light. *Catal. B-Environ.* **243**, 438–447 (2019).
12. Chen, X. et al. Confining energy migration in upconversion nanoparticles towards deep ultraviolet lasing. *Commun.* **7**, 10304 (2015).
13. Zheng, K. et al. Rewritable optical memory through high-registry orthogonal upconversion. *Mater.* 1801726 (2018).
14. Shi, F., Wang, J., Zhang, D., Qin G. & Qin W. *Mater. Chem.*, **21**, 13413-13421 (2011).
15. Dawson, P. & Romanowsk, M. Excitation modulation of upconversion nanoparticles for switch-like control of ultraviolet luminescence. *Am. Chem. Soc.* **140**, 5714–5718 (2018).
16. C. et al. Li^+ ion doping: an approach for improving the crystallinity and upconversion emissions of $NaYF_4$:Yb^{3+},Tm^{3+} nanoparticles. *Nanoscale* **5**, 8084–8089 (2013).

17. Wang, F. Wang, J. & Liu, X. Direct evidence of a surface quenching effect on size-dependent luminescence of upconversion nanoparticles. *Chem. Int. Ed.* **49**, 7456–7460 (2010).
18. Wang, F. et al. Tuning upconversion through energy migration in core–shell nanoparticles. *Mater.* **10**, 968–973 (2011).
19. Sun, T. et al. Integrating temporal and spatial control of electronic transitions for bright multiphoton upconversion. *Commun.* **10**, 1811 (2019).
20. Su, Q. et al. The effect of surface coating on energy migration-mediated upconversion. *Am. Chem. Soc.* 134, 20849–20857 (2012).
21. Wang, J. et al. Enhancing multiphoton upconversion through energy clustering at sublattice Level. *Mater.* **13**, 157–162 (2014).
22. Bansal, A. & Zhang, Y. Photocontrolled nanoparticle delivery systems for biomedical applications. *Chem. Res.* **47**, 3052–3060 (2014).
23. Jayakumar, M. K. G. Idris, N. M. & Zhang, Y. Remote activation of biomolecules in deep tissues using near-infrared-to-UV upconversion nanotransducers. *Natl. Acad. Sci. USA* **109**, (22), 8483–8488 (2012).
24. Dai, Y. et al. In vivo multimodality imaging and cancer therapy by near-infrared light-triggered trans-platinum pro-drug-conjugated upconversion nanoparticles. *Am. Chem. Soc.* **135**, 18920–18929 (2013).
25. Yao, C. et al. Near-infrared-triggered azobenzene-liposome/upconversion nanoparticle hybrid vesicles for remotely controlled drug delivery to overcome cancer multidrug resistance. *Mater.* **28**, 9341–9348 (2016).
26. Wang, Y., Liu, G., Sun, L., Xiao, J., Zhou, J. & Yan. C. Nd^{3+}-sensitized upconversion nanophosphors: efficient in vivo bioimaging probes with minimized heating effect. *ACS Nano* **7**, 7200–7206 (2013).
27. Xie, X., Gao, N., Deng, R., Sun, Q., Xu Q. H. & Liu, X. Mechanistic investigation of photon upconversion in Nd^{3+}-sensitized core–shell nanoparticles. *Am. Chem. Soc.* **135**, 12608–12611 (2013).
28. Liao, J., Jin, D., Chen, C., Li, Y. & Zhou, J. Helix shape power-dependent properties of single upconversion nanoparticles. *Phys. Chem. Lett.* **11**, (8), 2883–2890 (2020).
29. Wen, H. et al. Upconverting near-infrared light through energy management in core–shell–shell nanoparticles. *Chem. Int. Ed.* **52**, 13419–13665 (2013).
30. Wang, S. et al. Comparative investigation of the optical spectroscopic and thermal effect in Nd^{3+}-doped nanoparticles. *Nanoscale* **11**, 10220–10228 (2019).
31. Qin, W. et al. Ultraviolet upconversion fluorescence from ^6D_J of Gd^{3+} induced by 980 nm excitation. *Lett.* **33**, 19 (2008).
32. Pollnau, M., Gamelin, D. R., Lüthi, S. R., Güdel, H. U. & Hehlen, M. P. Power dependence of upconversion luminescence in lanthanide and transition-metal-ion systems. *Rev. B* **61**, 3337 (2000).
33. Pokhrel, M., Valdes, C. & Mao, Y. Ultraviolet upconversion enhancement in triply doped $NaYF_4$:Tm^{3+},Yb^{3+} particles: the role of Nd^{3+} or Gd^{3+} co-doping. *Mat.* **58**, 67e75 (2016).

34. Zhu, Q. et al. Yb^{3+}-sensitized upconversion and downshifting luminescence in Nd^{3+} ions through energy migration. *Dalton Trans.* **47**, 8581 (2018).
35. Rocha, U. et al. Nd^{3+} doped LaF_3 nanoparticles as self-monitored photo-thermal agents. *Phys. Lett.* **104**, 053703 (2014).
36. Wen, S., Zhou, J., Zheng, K., Bednarkiewicz, A., Liu, X. & Jin, D. Advances in highly doped upconversion nanoparticles. *Commun.* **9**, 2415 (2018).
37. Wang, F., et al. Microscopic inspection and tracking of single upconversion nanoparticles in living cells. *Light Sci. Appl.* **7**, 18007–18007 (2018).
38. Zhou, J., Chizhik, A. I., Chu, S. & Jin, D. Single-particle spectroscopy for functional nanomaterials. *Nature* **579**, 41–50 (2020).

Scheme

Scheme 1 is available in the Supplementary Files

Figures

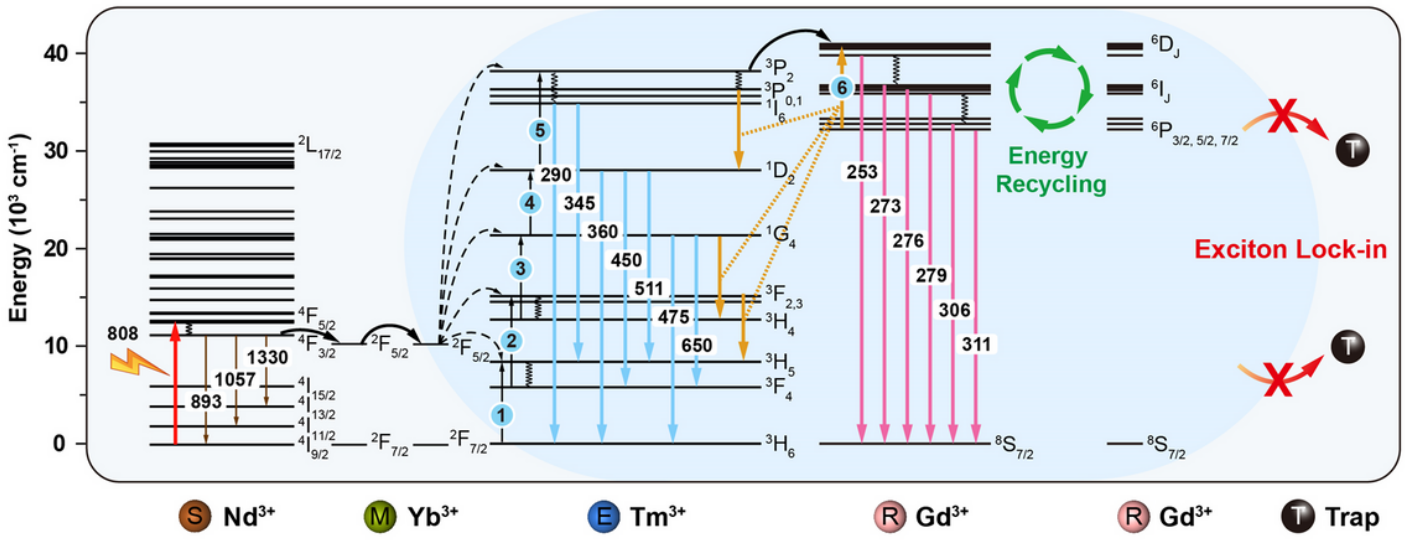

Figure 1

Schematic energy diagram of heterogeneously doped lanthanide ions and their cascade energy transfer within a core-multishell nanoparticle. When the nanoparticles are excited under 808 nm, Nd3+ sensitizers first absorb the excitation energy and pass onto Yb3+. Subsequently, the 3P2 state of Tm3+ is populated by a sequential five-photon energy transfer from the network of excited Yb3+ ions and relax to 3P0.1. The 6DJ state of Gd3+ is further populated via a six-photon energy transfer process. The inert NaYF4 layer can lock-in the Gd3+ excitation energy and then reuse the energy that would otherwise be depopulated by deleterious energy traps within the nanoparticles, resulting in upconversion emission in deep-UV region.

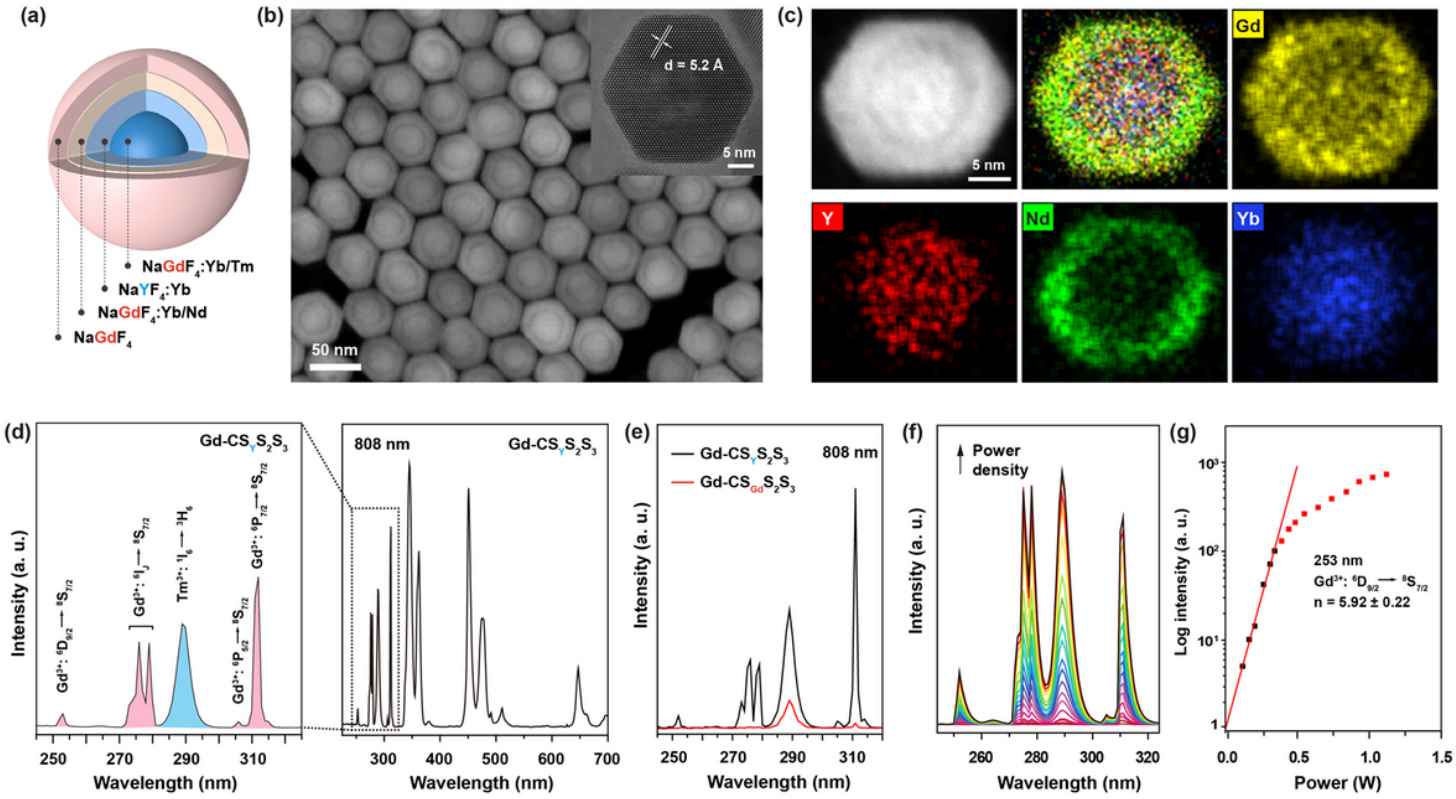

Figure 2

Structural and optical characterizations of Gd-CSYS2S3 nanoparticles before and after cation exchange. (a) Schematic illustration of the as-synthesized Gd-CSYS2S3 nanoparticles. (b) high-angle annular dark-field scanning transmission electron microscopy (HAADF-STEM) image and high-resolution TEM image of the corresponding nanoparticles (inset). (c) HAADF-STEM image and elemental mapping of a single Gd-CSYS2S3 nanoparticle, indicating the spatial distribution of the Gd, Y, Nd, and Yb elements in the core-multishell structure. (d) Room-temperature emission spectra of Gd-CSYS2S3 nanoparticles in cyclohexane under 808 nm excitation. (e) Emission spectra of Gd-CSYS2S3 and Gd-CSGdS2S3 under excitation of 808 nm CW diode laser. The excitation power density is 10 W cm-2. (f) Excitation-power-dependent UV upconversion emission spectra of Gd-CYS2S3 nanoparticles under 808 nm excitation. (g) Log intensity-pump power of the 253 nm upconversion emission of Gd-CYS2S3 nanoparticles.

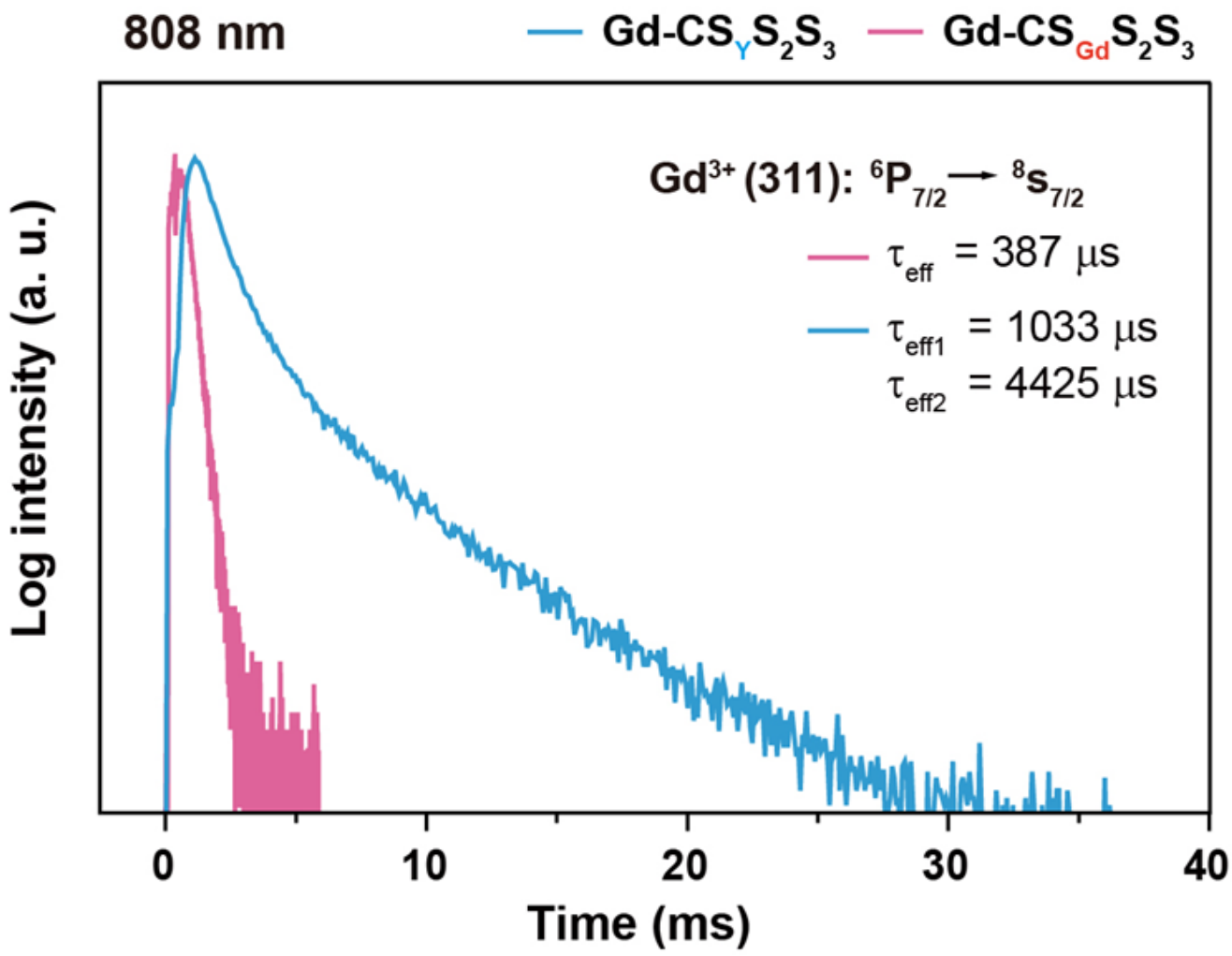

Figure 3

Lifetime decay analysis. Upconversion luminescence decay curves of Gd3+ emissions at 311 nm from Gd-CSYS2S3 v.s. Gd-CSGdS2S3 by pulsed 808 nm excitation.

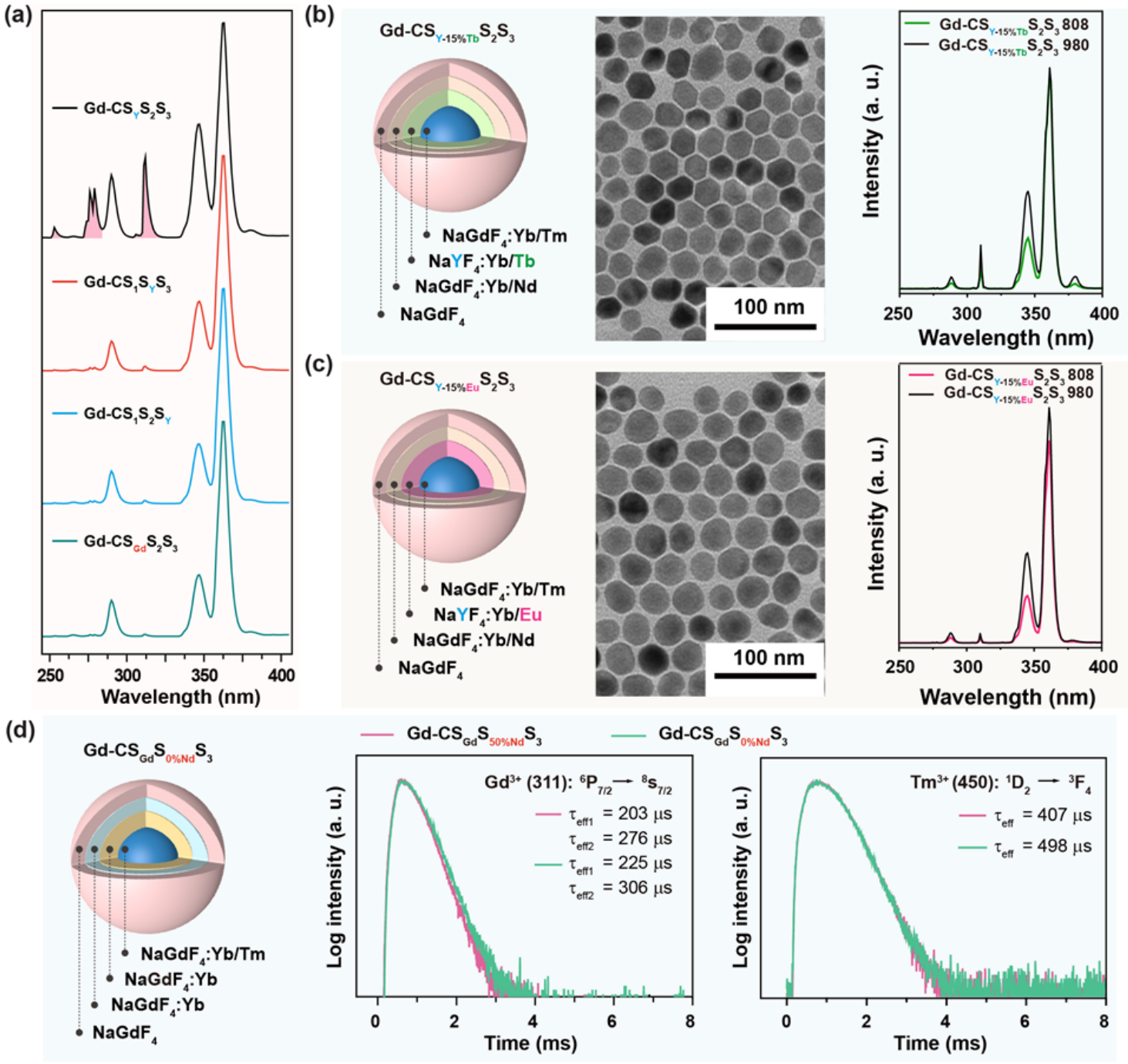

Figure 4

Characterization of core-multishell nanoparticles with alternative dopants and structural layouts. (a) Room-temperature upconversion emission spectra of solutions containing Gd-CSYS2S3, Gd-CS1SYS3, Gd-CS1S2SY and Gd-CSGdS2S3 nanoparticles under 808 nm excitation at a power density of 10 W cm−2. (b,c) Schematic illustration, TEM images and photoluminescence spectra of the as-synthesized Gd-CSY-15%TbS2S3 and Gd-CSY-15%EuS2S3 nanoparticles. (d) Schematic illustration of the as-synthesized Gd-CSGdS0%NdS3 nanoparticles, and the upconversion luminescence decay curves of Gd3+

emission at 311 and Tm3+ emission at 450 nm of Gd-CSGdS50%NdS3 and Gd-CSGdS0%NdS3 nanoparticles under 980 nm excitation, respectively.

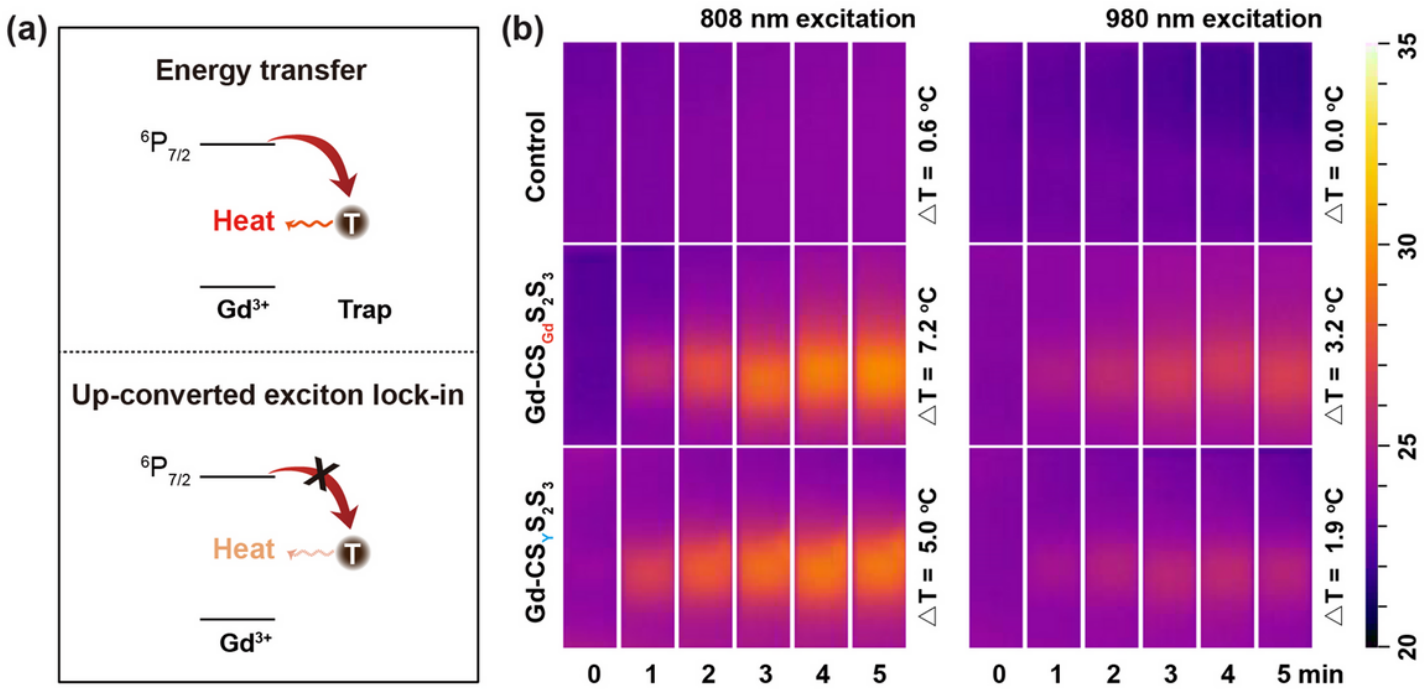

Figure 5

Schematic illustration and infrared thermal images of Gd-CSGdS2S3 and Gd-CSYS2S3. (a) Schematic illustration of generated heat induced by conventional energy transfer and upconverted exciton lock-in mechanism. (b) Infrared thermal images of cyclohexane solutions of Gd-CSGdS2S3 and Gd-CSYS2S3 under continuous irradiation with 808 nm and 980 nm laser (power density of 10.0 W cm−2) for 5 min.

Supplementary Files

This is a list of supplementary files associated with this preprint. Click to download.

- Scheme1.png
- UpconvertedExcitonLockinforDeepUltravioletEnhancementSI.doc